The top-bottom iV-beam phase contrast effect from finite crystals II. Theory

P. Goodman [a] , A. E. C. Spargo [a] , L. C. Qin [b] & K. Ishizuka [c]

[a] School of Physics, University of Melbourne, Parkville, Victoria, 3052,
Australia

[b] Institute of Metal Research, Academia Sinica, 110015, Shenyang, P.R.
China

[c] Institute for Chemical Research, Kyoto University, Iji, Kyoto-Fu, 611,
Japan

Available online: 13 Sep 2006

PLEASE SCROLL DOWN FOR ARTICLE

The top–bottom *N*-beam phase contrast effect from finite crystals II. Theory

By P. Goodman, A. E. C. Spargo

School of Physics, University of Melbourne, Parkville, Victoria 3052, Australia

L. C. Qin

Institute of Metal Research, Academia Sinica, 110015 Shenyang, P.R. China

and K. Ishizuka

Institute for Chemical Research, Kyoto University, Iji, Kyoto-Fu 611, Japan

ABSTRACT

The top–bottom contrast effect which has been observed in dark-field images of aperiodic surface detail and which was discussed in Part I is shown to arise as a result of *N*-beam refraction reversal in one or more of the important Bloch wave components, formed by high-energy transmission electron diffraction. The effect is shown to arise in two-beam as well as *N*-beam diffraction. In particular, the zero-contrast condition, whereby the contrast from one or other surface is suppressed, and found experimentally in Part I, is found to arise as a consequence of a finite-crystal Bloch wave degeneracy.

§1. INTRODUCTION

The specialised development of the dynamic theory for application in electron microscopy is not particularly suited to the calculation or understanding of scattering from finite polyhedral crystals or crystals with three-dimensional aperiodic features. This is because the two most used treatments—physical optics (Cowley and Moodie 1957) and Bloch wave expansion (Bethe 1928, Fujimoto 1959)—assume plane-parallel boundary conditions and infinite periodicity respectively from the outset.

Dynamic scattering by crystals finite in three dimensions has usually been treated as a separate subject and directed towards interpreting diffraction fine structure rather than the real-space image. Thus Kato's (1952) analysis of the two-beam diffraction fine structure was made for isolated crystal wedges. This treatment permits a comparison with diffraction observations (for example Cowley, Goodman and Rees (1957)), provided that the diffraction spot components are treated as discrete points, but is not capable of yielding microscope contrast for the line boundaries separating neighbouring crystal faces in projection, since diffuse scattering and coherent interference are explicitly excluded. Fujimoto's (1965) finite-crystal treatment for *N*-beam diffraction did include diffuse scattering but was applied only to the case of a spherical crystal, without solving the problem of polygonal boundary conditions.

The aim of the present paper is to extend Kato's treatment to allow interpretation of dark-field microscope contrast obtained from polygonal crystals, including the top–bottom contrast effect (Goodman and McLean 1976), and further to provide a basis for understanding the more recent imaging of surface steps by high-resolution dark-field microscopy which was presented in Part I in the present series (Goodman and Warble 1987).

206   P. Goodman *et al.*

§ 2. GEOMETRIC OPTICS

Figure 1 shows the passage of parallel illumination through a refracting object of triangular cross-section. The post-object planes corresponding to negative and positive defects of focus, Δf_- and Δf_+, are seen to give dark and bright images of the apex respectively, for *both* orientations (apex up and apex down) of the triangle. Figure 1 serves to show the optical origin of apex contrast in out-of-focus microscope images without resorting to diffraction.

Introducing diffraction, even kinematically, allows us access to the crystal shape transform in the vertical direction, so that by changing the excitation error ζ from positive through zero to negative values we must generate a top–bottom effect, at least in phase, in the diffracted beam (Goodman and McLean 1976). Further interpretation of top–bottom reversal, in intensity, has been given recently in qualitative form by Fujimoto and Goodman (1988) using the weak-coupling approximation. It is now of interest to find the simplest exact dynamical scattering solution which predicts this observation and, as a first step, to re-examine the original two-beam solution of Kato.

§ 3. EXTENSION OF KATO'S THEORY

In Kato's (1952) paper the diffraction-doublet fine-structure produced by individual crystal wedge segments of the finite-MgO-crystal cube were treated independently. By allowing beams transmitted through neighbouring crystal segments to interfere coherently in an image plane this unnecessary restriction can be removed, and the possibility of top–bottom contrast explored, using the concept of contrast inversion illustrated in fig. 1.

Figure 2 shows the two-beam dispersion surface constructions for diffraction from a triangular crystal cross-section for the two cases of apex up and apex down, with the resulting emerging vacuum wave-vectors K_0 and K_g, for both positive and negative excitation error ($\zeta > 0$ and $\zeta < 0$). The results given in fig. 2 show that, while inversion of the sign of excitation error leads to an inversion of contrast in both beams, only the

Fig. 1
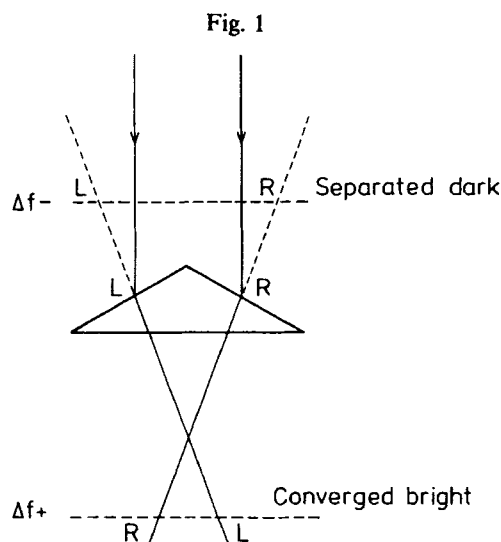
Ray optics formation of negative and positive defect-of-focus images for a positively refracting prism.

$\mathfrak{g}_g^{-}$

Fig. 2

CRYST. G

VAC. G

CRYST. O

VAC. O

1

2

L   R

f_s

R1

L2

L2 R1

R2

L1

L1 R2

L   R
● ●
2   1

L   R
● ●
1   2

L   R
● ●
2   1

L   R
● ●
1   2

G

O

(a)

P. Goodman *et al.*

(b)

(c)

P. Goodman *et al.*
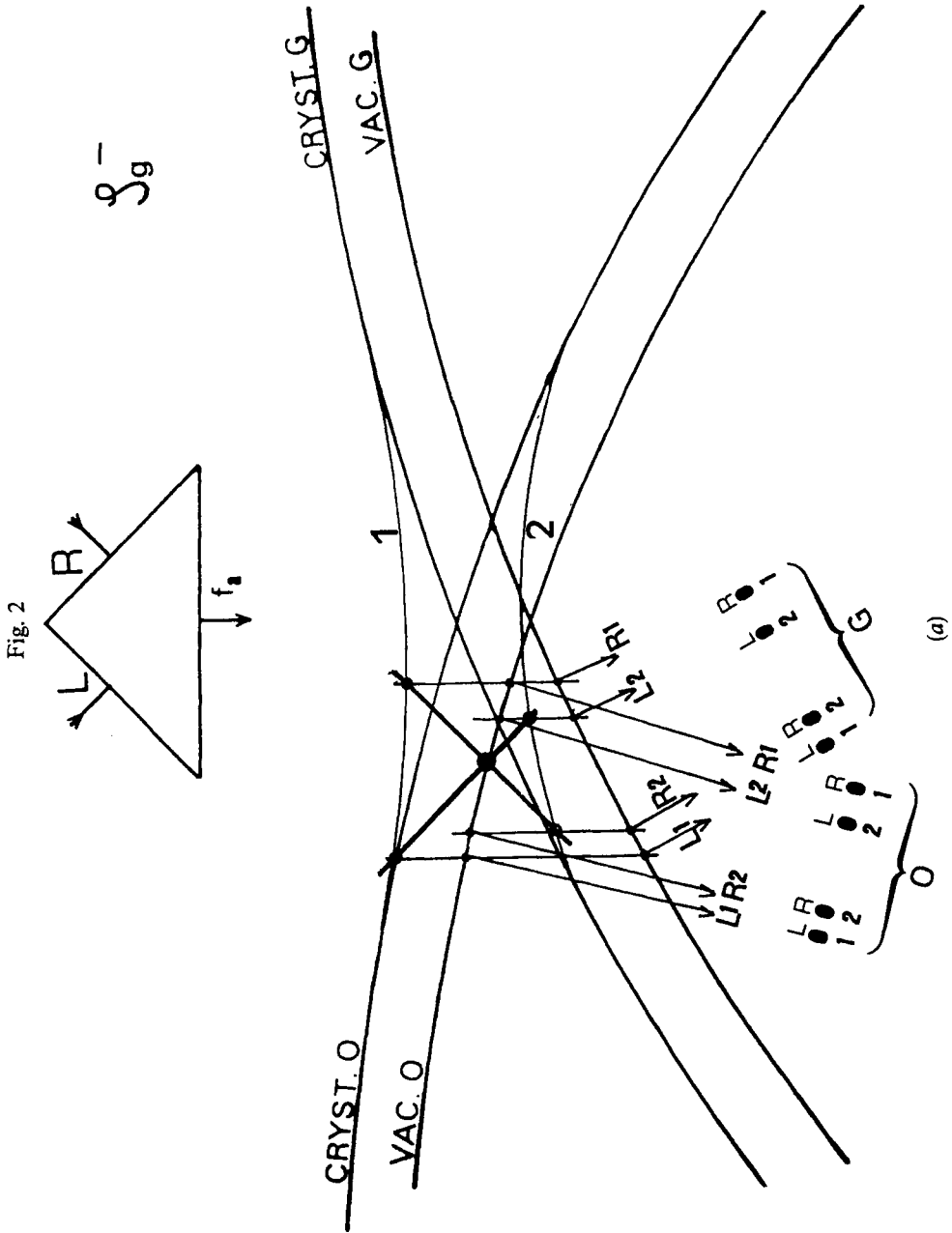
Dispersion surface construction for two-beam diffraction from a crystal of triangular cross-section, with (*a*) apex up, ζ_g negative; (*b*) apex up, ζ_g positive; (*c*) apex down, ζ_g negative; (*d*) apex down, ζ_g positive. The braces show the collected fine-structure for the O and G beams.

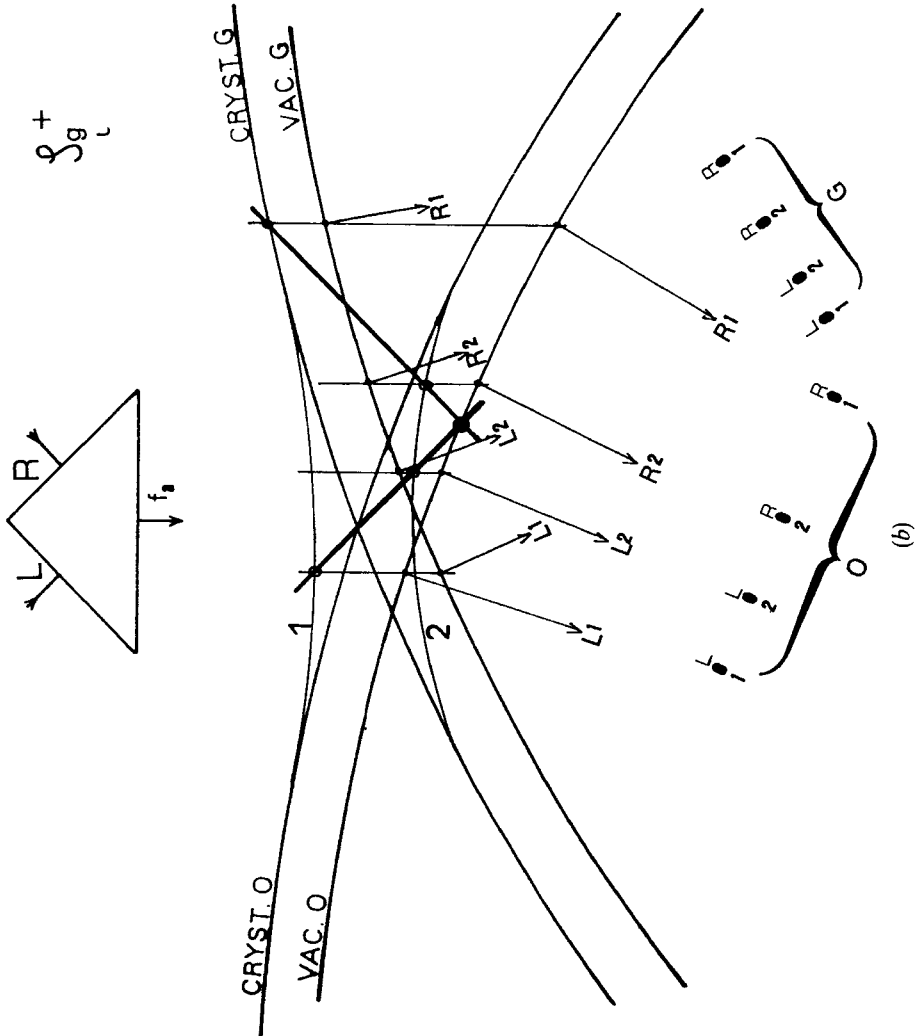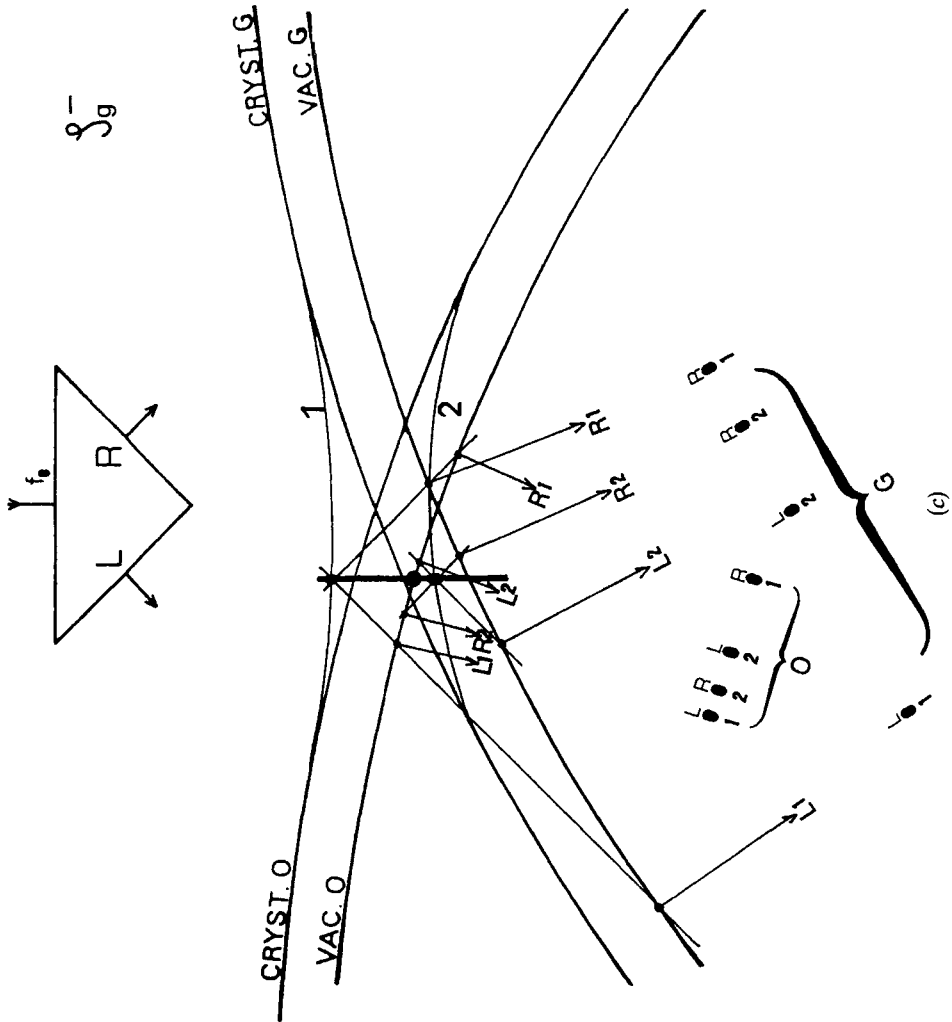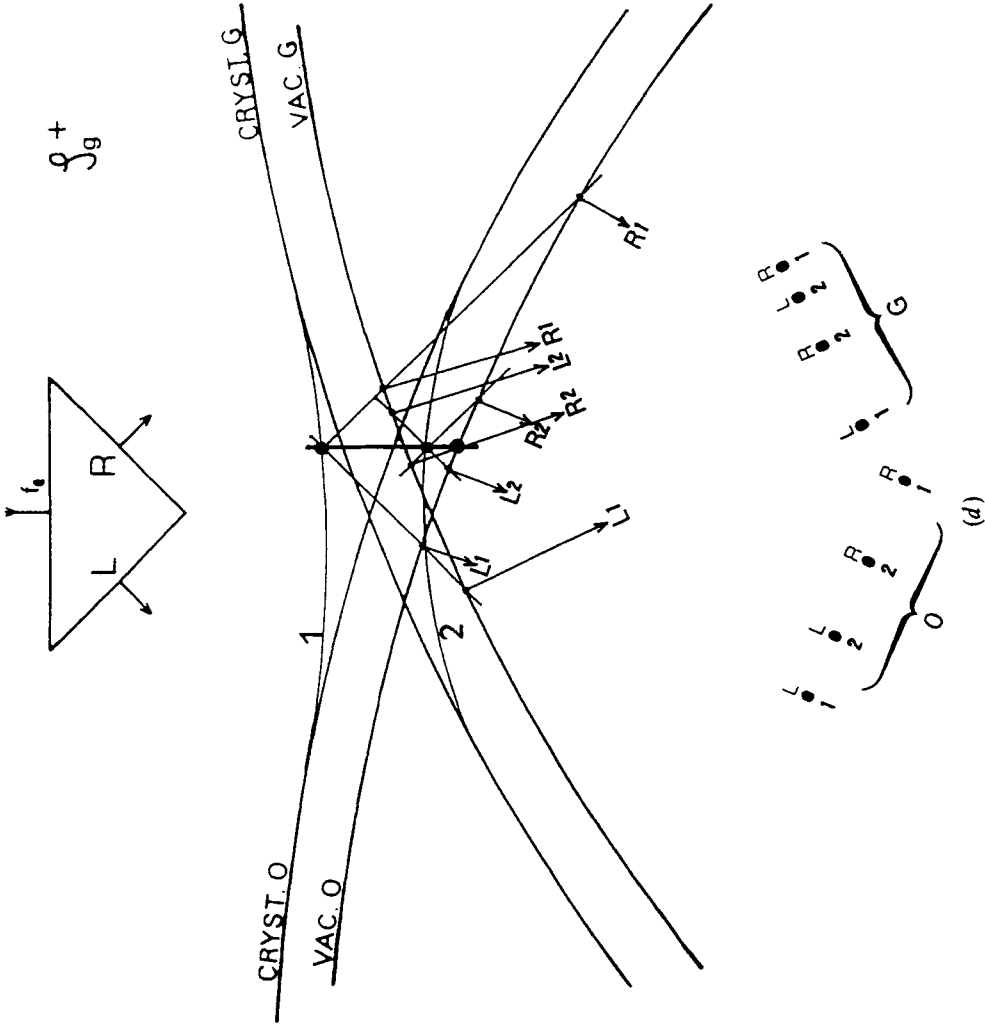diffracted beam G exhibits a contrast inversion with inversion of the crystal about the axis perpendicular to the page; that is only the G beam exhibits a top–bottom effect, in agreement with observation (Goodman and McLean 1976). The analysis shows that this effect is attributable to Bloch wave 2. Bloch wave 1 has invariant optical properties with respect to the sign of the excitation error ζ. Since this Bloch wave, which peaks on atom sites, is more heavily absorbed, an effect arising from Bloch wave 2 should be observed at moderate crystal thicknesses. In addition, a relative change in position occurs in the fine structure with changing ζ_g. The results, summarised in the table, show that Bloch wave 2 components move from inner to outer position in the array at large negative values of ζ.

An interesting point which arises from the inversion of Bloch wave 2 with ζ is that at a particular value (not necessarily $\zeta = 0$) the two components, from left- and right-hand crystal facets, emerge parallel, corresponding to coincident positions in the fine structure. This gives rise to a 'zero-contrast' condition where contrast for the crystal edge will be zero for this Bloch wave irrespective of focus value Δf.

This behaviour carries over into the zone axis case. Blume (1966) showed that, at the [111] zone axis, symmetry reduces the seven-beam to a two-beam dynamic interaction. This reduction, which in the vicinity of the zone is sensitive to the exact orientation and from observations is effectively two- or three-beam in character, simplifies the analysis.
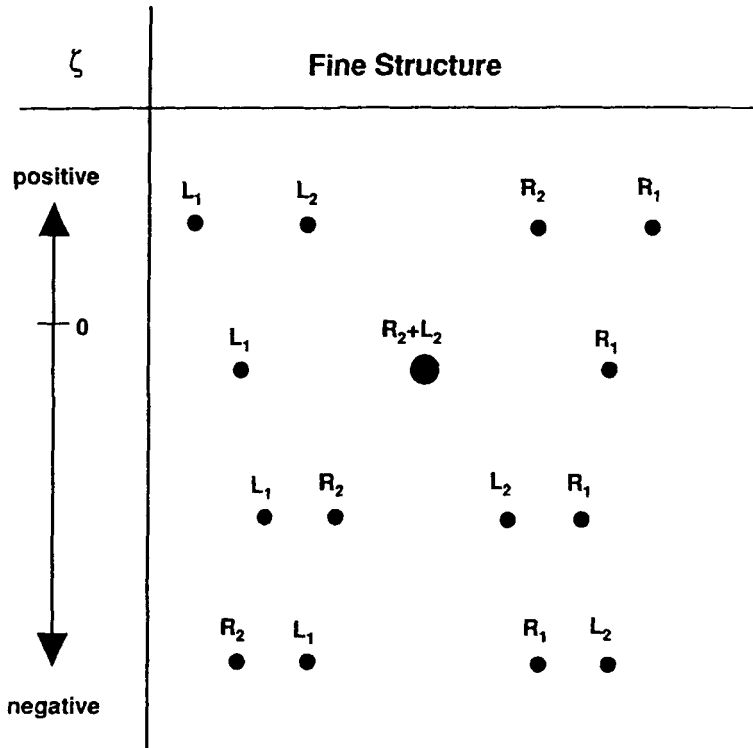
Change in the relative disposition of fine-structure components as a function of excitation error ζ, derived from the construction in figs. 2(a) and (b) over an extended ζ range. Fine-structure arrays for the G beam are shown diagrammatically in the second column, for increasingly negative values of ζ from top to bottom. R_2, L_2, R_1 and L_1 have the same meanings as in fig. 2.

Figure 3 shows diagrammatically the relevant symmetry-reduced dispersion surface constructions in simplified and schematic form for the combinations of crystal orientation and excitation error sign as in fig. 2. Only a one-third segment of a [111]-oriented MgO cube needs to be considered since the crystal has trigonal symmetry in this orientation. This segment has two neighbouring facets forming an apex on either the entrance or the exit face, labelled e and a respectively in the upper diagrams of each part of the figure. Diffraction fine structure is derived for the H (220) beam in each case. Figures 3 (a) and (c) illustrate the exact [111] zone-axis orientation for which ζ_{220} is negative, while figs. 3 (b) and (d) represent the situation holding at a second orientation, depicted in fig. 4, of a simultaneous five-beam excitation, for which ζ_{220} is positive. Appropriate choice of the parameter V_H/V_O causes the 'zero-contrast' condition to appear in both orientations, in association with the opposite sign of excitation error for the beam H. Thus fig. 3 (a) shows this condition arising in Bloch wave 2 (assumed to be the strongest Bloch wave), owing to coincidence of the waves from faces e_L and e_R. In fig. 3 (b) these two waves (now from faces a_L and a_R) are separated by refraction. Similarly, figs. 3 (c) and (d) show this situation in reverse, since the diffraction space or ray form of reciprocity (Pogany and Turner 1968) relates figs. 3 (a) and (d) and figs. 3 (b) and (c) with respect to the H beam. The lack of complete equivalence is shown as a difference in slope of the intersected H-beam vacuum sphere within each of the near-equivalent pairs. This illustrates the point that, in order to obtain fine-structure (and dark-field image) equivalence, both reciprocal-space (Pogany and Turner 1968) and real-space (Cowley 1969) forms of reciprocity need to be invoked. Thus, for an inversion of the crystal, a change in excitation error sign needs to be combined with an inversion of microscope optics, achieved by changing from transmission electron microscopy to scanning transmission electron microscopy (or *vice versa*) to obtain the reciprocity-related wavefunction.

§4. Comparison with experiment

Figure 3 predicts a top–bottom effect arising in the H-beam dark-field image as a consequence of the fine-structure splitting and coalescing for Bloch wave 2. These predictions can be followed by electron diffraction and microscopy of the MgO[111] cube. Experimental observations were made using a JEOL 100CX side-entry electron microscope. Figure 5 (a) shows the diffraction pattern from MgO cube in near-[111] orientation. The six 220-indexed reflections show trigonal fine-structure splitting. At low magnifications (fig. 6 (a)) each fine-structure pattern appears to be composed of three bright dots at the corners of a triangle. These dots may be considered as the almost-superimposed components of the Bloch wave 2 fine structure, corresponding to the case in fig. 3 (a). The separated dots then correspond to the dispersed case in fig. 3 (b). This simplified interpretation is shown schematically in fig. 5. In fig. 6 (b) the enlargement of one fine-structure formation shows that the actual distribution is somewhat more complicated, with additional fine-structure components along the sides of the triangle. Additionally, the diffraction pattern was taken with an unavoidable slight deviation from the exact [111] setting.

Figure 7 shows the equivalent dark-field images from a 220-indexed reflection with the orientation very close to [111]. The sequence of three images are for substantial negative, almost zero and substantial positive defects of focus in figs. 7 (a), (b) and (c) respectively. In this sequence it is seen that one of the trigonally disposed set of crystal surface edges gives almost zero contrast at all values of defocus, that is the *pendellösung* fringes continue without intensity change through the 120° angle; these were later

Fig. 3

(a)

(b)

(c)

(d)
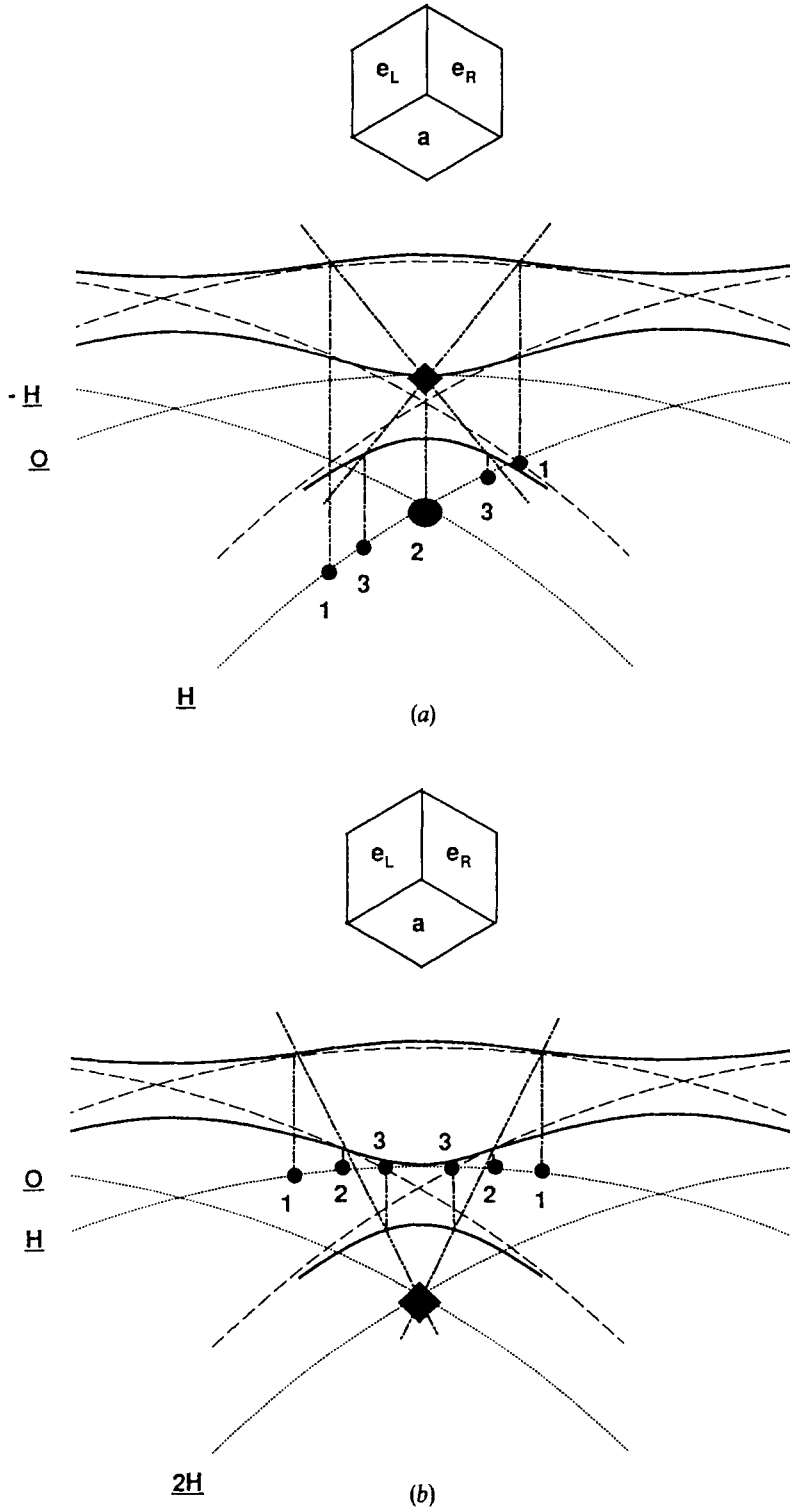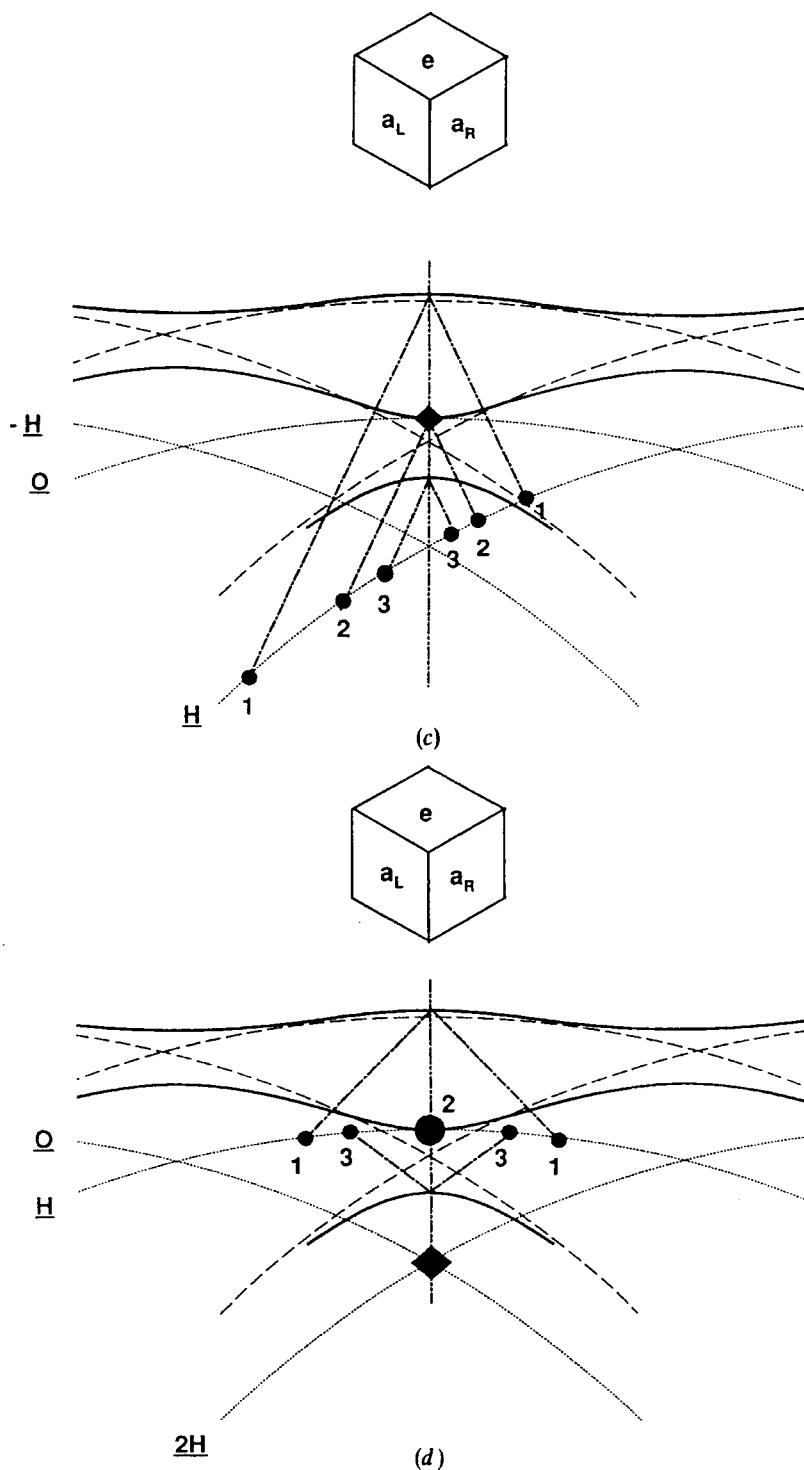
Two-dimensional representation of the symmetry-reduced diffraction from the three-dimensional cube segment shown: ◆, Laue point; ●, origin of H-beam wave-vectors; ·······, vacuum spheres; – – –, crystal spheres; ——, dispersion surface; — — —, entrance (e) surface normal; ———, exit (a) surface normal. (a)–(d) show the four cases of apex up and apex down for (a),(c) orientations of exact zone-axis orientation (ζ_H negative) and (b),(d) the complementary orientation of simultaneous excitation of five reflections (ζ_H positive), which is depicted in fig. 4.
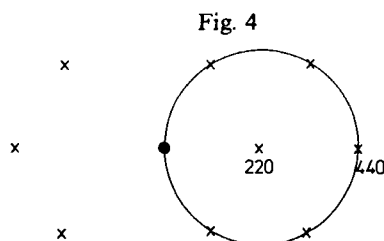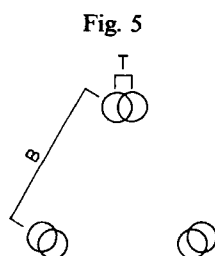
Fig. 4

Diagram showing Laue circle around the 220-indexed G beam for the second complementary orientation in fig. 3.

Fig. 5

Idealised representation of the triangular fine structure in fig. 6 (*b*). B and T represent the non-collinear displacements involved in the three-dimensional interpretation of fig. 3 with respect to Bloch wave 2. The near-coalescence for waves emerging from one crystal surface and the finite dispersion for the reverse surface are represented by the square brackets T and B respectively.

identified as top-surface edges by rotating the specimen and observing top–bottom parallax. Then, the complementary bottom-surface contrast goes from dark through zero to bright enhancement, at the trigonal [100]-directed edge lines, in the sequence fig. 7 (*a*), (*b*), (*c*). *Pendellösung* fringes are still present along these lines but are phase shifted for $\Delta f \neq 0$; that is in fig. 7 (*c*) with Δf positive the first bright fringe is shifted towards the vacuum edge. This shift is expected from the geometry of fig. 1; since the left- and right-hand image shift vectors are perpendicular to this line of contrast and the projected wedge shape is triangular, the *effective* crystal thickness undergoes a jump from zero to a finite value along this line. The zero-contrast and finite contrast behaviour seen in the dark-field images are in agreement with the dispersion surface predictions given from fig. 3.

## § 5. APPLICATION TO HIGH RESOLUTION

In this paper we have set out to explain the origin of top–bottom phase contrast in *N*-beam diffraction, and especially to explain phenomena associated with high-resolution dark-field images of surface structures as described in Part I. In this latter study, both types of top–bottom contrast effect discussed above were observed, with different diffraction conditions, that is both black-to-white contrast reversal with change in excitation error sign (Part I, fig. 5), and the complete suppression of contrast from one or other surface for one sign of excitation error (Part I, fig. 6 (*b*)).

From the analyses given above, we find that both these top–bottom phenomena—contrast reversal and contrast disappearance—can be identified for low-magnification
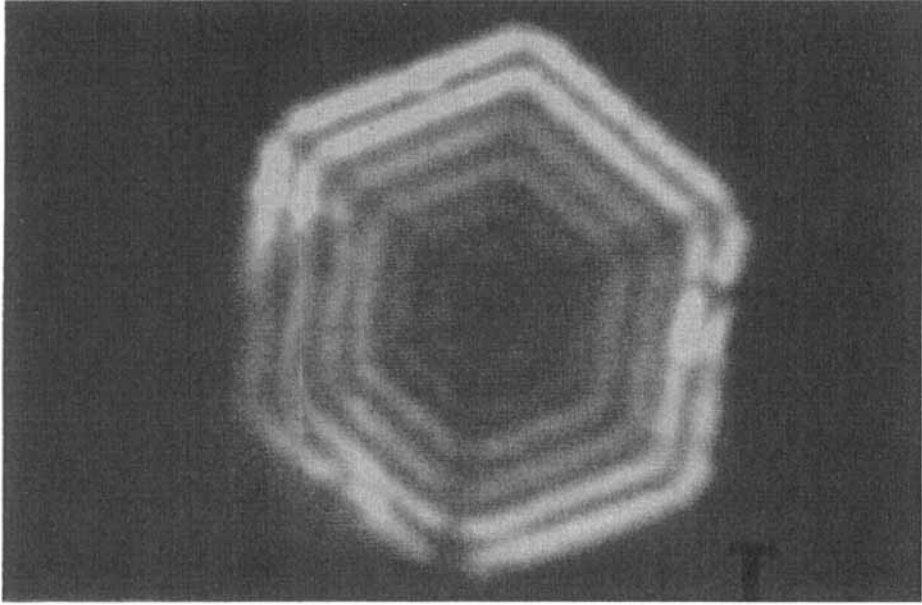
P. Goodman *et al.*
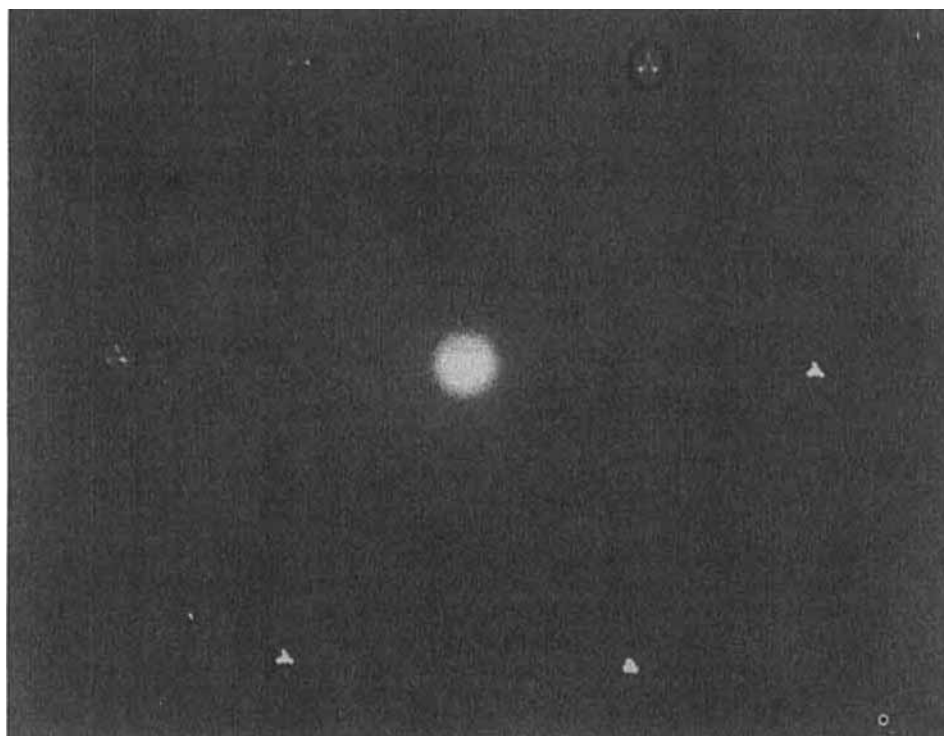
Fig. 6

(a)
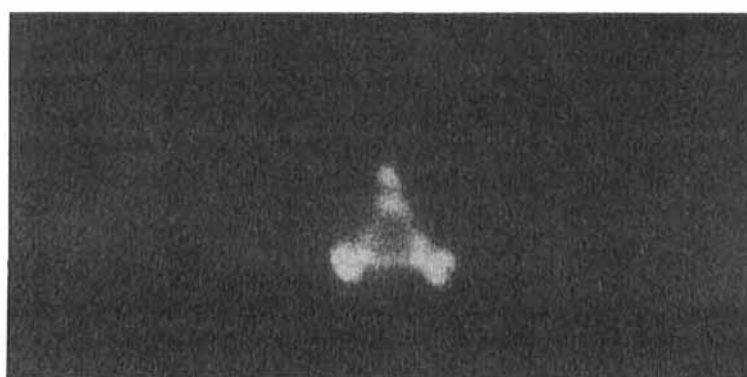
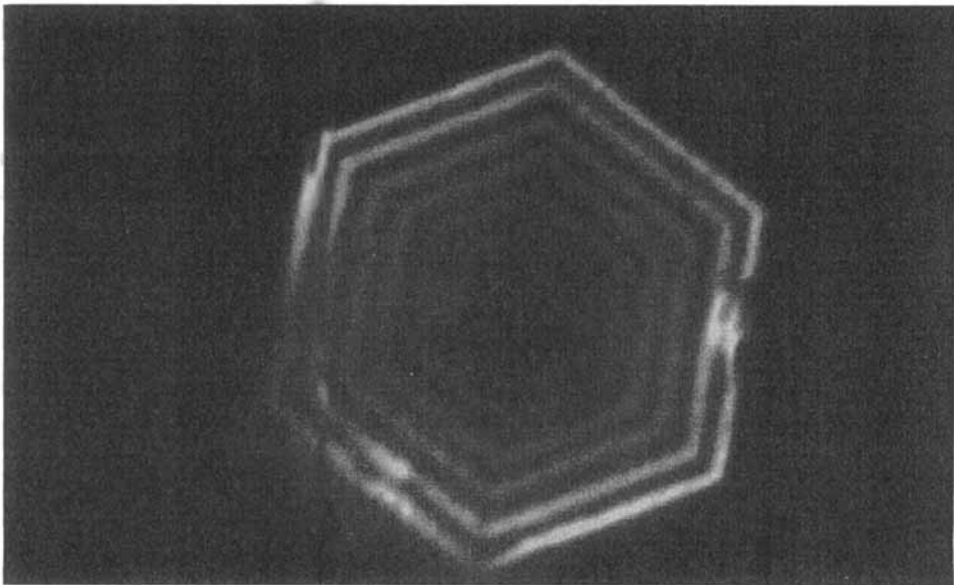

(b)

Diffraction pattern from a [111]-oriented MgO cube; (a) complete pattern, with one 220-indexed reflection encircled; (b) encircled reflection from (a) enlarged.
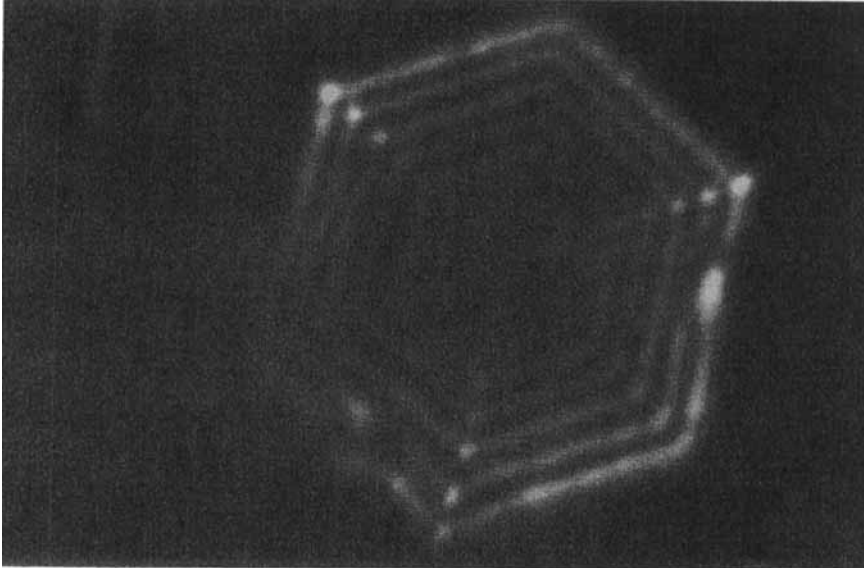
Fig. 7

(a)

(b)

(c)

Dark-field images of the cube giving the pattern of fig. 6. (a), (b) and (c) are taken with Δf negative, zero and positive respectively. The [100]-directed cube edge marked T in the images has been identified as located on the top or beam-entry side of the crystal.

images treated as the Fourier transform of the diffraction fine structure. The importance of diffuse scattering generated by the specific surface detail being imaged becomes of increasing relevance at higher magnifications. To generalise the results obtained from a Kato-type description based on discrete diffraction fine-structure components, it is only necessary to allow streaks of appropriate structure to replace spots in the fine structure. The arguments used here are then not materially altered; where previously we had an interchange of L and R spots we now have a reversal of a Fresnel fringe extending continuously between the former spot positions, for a particular Bloch wave index.

Using the terminology in Part I (eqn. (2)), the wavefunction at a point x, y of the dark-field image is given by

$$\Psi_h^{x,y} = \langle S_a | Q | S_e \rangle, \tag{1}$$

where S_a and S_e are integrals over exit and entrance surfaces respectively and Q is the bulk crystal operator. The ith Bloch wave component is then

$$\Psi_h^i = Q | S_e \rangle,$$

with

$$S_e = \int_s \frac{1}{\delta} f_s \exp(-ik\delta) \, ds.$$

The Fresnel integral S_e is non-zero owing to the finite scattering power f_s into the small-angle scattering regime of local surface structure at points $s = s_1$. The Fresnel fringe has a finite width at a finite depth δ, which can then be taken as the initial condition for Q. This artificial division of depth into surface and bulk, which is needed for the formalism

ot eqn. (1), allows us to estimate a minimum crystal thickness for which a top–bottom effect is likely to be detectable. Setting a resolvable fringe width at 0·5 nm leads to a minimum depth of around 20 nm for 200 kV electrons required to achieve useful top–bottom differentiation.

Finally, attention needs to be given to the situation holding when surface steps have vertical faces which are almost parallel to the incident beam direction. This situation occurs frequently, for example, in examining steps in MgO surfaces at high resolution (Part I). In this case the forward-scattering small-angle approximation is no longer valid; as in low-energy electron diffraction and reflection high-energy electron diffraction, 90° incidence, whereby a significant amount of energy is lost to the forward-diffracted beam, can occur with the onset of evanescent propagation. From a very simple analysis, this condition will occur for steps on the entrance face only and will be accessed for positive rather than negative values of excitation error for reflections near the MgO[001] zone axis. In this case, one would expect defect or black-line contrast to occur at vertical-step sites in the dark-field image. This mechanism may well be important in enhancing contrast from entrance-surface detail at high resolution; a more complete and numerical evaluation would be needed to determine the relative importance of 'surface resonance' to the observed top–bottom contrast enhancement.

§6. CONCLUSIONS

From the above sections, we find that the theory can be developed at two levels, that is that involving ray optics and with neglect of Fresnel diffraction and at the better approximation required by high-resolution microscopy (Part I), to allow for Fresnel diffraction from surface apices. The change to considering diffuse scattering involves no additional theoretical principles, but the simpler approach in which this is neglected implies that the ray form of reciprocity (Pogany and Turner 1968) applies with sufficient approximation to the dark-field micrographs. This is seen from experimental evidence to be true at very low magnifications. At higher resolutions the more complete form which includes Fresnel optics reciprocity (Cowley 1969) is seen to be operative in removing any equivalence between reversing excitation error sign and inverting the crystal in the same instrument.

The present analysis differs from earlier interpretations (e.g. Part I) in being an accurate N-beam treatment to the first order; that is the approximation has been to neglect weak-beam interactions but to include interactions between the main diffracted beams using symmetry reduction at the zone-axis setting. With this approximation, the zero-contrast effect applying to one surface rather than the other can be interpreted in terms of a finite-crystal Bloch wave degeneracy.

The present discussion is valid only with respect to the forward-scattering (small-angle) approximation. Further consideration has to be given to include large-angle diffuse scattering from vertical crystal facets. However, it is interesting to note that progress this far is possible because of the present-day confidence in the applicability of the Fresnel formalism to high-voltage electron microscopy within the forward-scattering approximation. At the time of the initial theory (Kato 1952), lack of accumulated data confirming the validity of this approximation, which allows simple incorporation of nonplanar boundary conditions (particularly those relating to surface having discontinuities in gradient), was not available.

REFERENCES

BETHE, H. A., 1928, *Annln. Phys.*, **87**, 55.
BLUME, J., 1966, *Z. Phys.*, **191**, 248.
COWLEY, J. M., 1969, *Appl. Phys. Lett.*, **15**, 58.
COWLEY, J. M., GOODMAN, P., and REES, A. L. G., 1957, *Acta crystallogr.*, **10**, 19.
COWLEY, J. M., and MOODIE, A. F., 1957, *Acta crystallogr.*, **10**, 609.
FUJIMOTO, F., 1959, *J. phys. Soc. Japan*, **14**, 1558; 1965, *Z. Naturf.* (a), **20**, 367.
FUJIMOTO, F., and GOODMAN, P., 1988, *Acta crystallogr.* A, **44**, 960.
GOODMAN, P., and McLEAN, J. D., 1976, *Phil. Mag.*, **34**, 861.
GOODMAN, P., and WARBLE, C. E., 1987, *Phil. Mag.* B, **56**, 15.
KATO, N., 1952, *J. phys. Soc. Japan*, **7**, 397.
POGANY, A. P., and TURNER, P. S., 1968, *Acta crystallogr.* A, **24**, 103.